京都大学防災研究所年報 第 67 号 B
DPRI Annuals, No. 67 B, 2024

Weather Modification Simulation of Line-Shaped Convective System Torrential Rainfall by Introducing Offshore Curtain

Kosei YAMAGUCHI, Shoma NISHIMURA(1) and Eiichi NAKAKITA

(1) Graduate School of Engineering, Kyoto Univ.

Synopsis

There is concern that heavy rainfall is becoming more serious as global warming progresses, and it is hoped that heavy rainfall can be mitigated through weather control. Therefore, we would like to consider developing a weather control device as a wind resistor (i.e., Offshore Curtain) by raising a huge kite over the ocean and suspending a huge curtain-like membrane body on the kite. The objective of this study is to investigate whether it is possible to suppress heavy rainfall by manipulating winds to simulate Offshore Curtain through numerical simulations. The meso-scale meteorological model CReSS (Tsuboki and Sakakibara, 2002) was used for the numerical simulation of the heavy rainfall. The results indicate that the maximum intensity of line shaped convective rainfall can be reduced by up to 34%. In addition, sensitivity experiments were conducted by varying the altitude and horizontal position of the Offshore Curtain, and the rainfall suppression effect varied from -34.0% to +19.2%.

Keywords: Weather Control, Line Shaped Convective System, Offshore Curtain

1. Introduction

In recent years, torrential rainfall disasters that cause extensive damage have been occurring frequently, and one of these disasters is caused by the line-shaped convective rainfall. In the afternoon of July 5, cumulonimbus clouds formed one after another in Fukuoka Prefecture and moved eastward while developing, forming a linear precipitation zone. As a result, 37 people were killed, 4 were missing. Under these circumstances, a new option of weather control is beginning to be considered. Yamaguchi et al. (2024) conducted a wind field control simulation for the Guerrilla-heavy rainfall and showed that the peak intensity of rainfall was suppressed by 27 %. Therefore, it is expected that the wind field manipulation will be able to suppress rainfall even for line-shaped convective rainfall. As for infrastructure facilities in the sky, Toyota Motor Corporation is conducting research and development of technology using big kites as part of Mothership project. If the device can be built in the sky above, it is expected that the infrastructure for weather control can be used to manipulate winds in the sky above.
The purpose of this study is to investigate by numerical simulation whether it is possible to control line-shaped convective heavy rainfall by manipulating the wind, assuming a wind manipulation device (i.e., Offshore Curtain; described in Chapter 4) to be installed above the sky.

2. Previous research about Rainfall Control

In this chapter, previous studies that have analyzed weather control and review the position of this study are discussed.

2.1 Control of guerrilla heavy rainfall

There are a few studies that attempt to control heavy rainfall. Yamaguchi et al. (2019), using their original computational model LES (Large-Eddy-Simulation), which can directly calculate eddy fluctuations larger than the computational grid, found that some of the eddy tubes rise above the ground surface and pointed out the possibility of suppressing heavy rainfall by weakening these eddy tubes, and Yamaguchi et al. (2024) used the LES model to represent the case of the 2008 Kobe-Toga river heavy rainfall that triggered the guerrilla rainfall research, and further manipulated the wind field to weaken the vortex pipe at the lower level. As a result, the maximum rainfall intensity was suppressed by about 27 %. In this study, the control rainfall event is line shaped convective systems.

2.2 Control of line shaped convective system

Yokoyama et al. (2015) confirmed that even relatively small-scale seeding with reduced spray volume and area can suppress the area maximum precipitation and time maximum precipitation and time maximum precipitation of line shaped convective system by 10-30 % by considering the area and time of onset of upwelling. In addition, the mechanism of rainfall suppression is that seeding during cumulonimbus development significantly suppresses the formation of hail due to the competitive growth of ice crystals (in which they compete for water vapor as they grow) and seeding in the early stage of cumulonimbus development suppresses hail formation because the precipitation particles that have grown due to seeding generate downdrafts as they fall. In addition, it has been shown that the seeding in the early stage of cumulus cloud formation causes downdrafts when the precipitation particles grown by seeding fall, and as a result, the upwelling at the peak is suppressed. Cloud seeding intervenes in the thermodynamic field but this study focuses on the inflow of water vapor and the dynamical structure of the line-shaped convective system and examines the possibility of controlling line-shaped convective system heavy rainfall by Offshore Curtain.

2.3 Effectiveness and Promotion Risks of Rainfall Control by Offshore Curtain

One of the requirements for meteorological control is the reduction of rainfall promotion risk. To quantitatively evaluate the effectiveness of rainfall suppression by strong cold method seeding used in the study by Yokoyama et al. (2015) and the reliability of seeding with respect to rainfall promotion risk, Yagi et al. (2017) conducted experimental numerical simulations to quantitatively evaluate the reliability of seeding focusing on the risk of rainfall acceleration. The results showed that in cases caused by linear precipitation zones, seeding in the upper layers of cumulus clouds showed a high suppression ratio of about 36 % and a low enhancement ratio of 5 %, indicating that strong cold method seeding in the upper layers of cumulus clouds is particularly effective in cases caused by linear precipitation zones. The results also indicate that the strong cold method of seeding in the upper layers of cumulus clouds is particularly effective in cases caused by linear precipitation bands. It was also confirmed that the weakening of vertical wind speeds leads to the suppression of precipitation. In this study, we evaluate the suppression effect and the promotion risk of line-shaped convective system heavy rainfall through sensitivity experiments of wind field manipulation assuming Offshore Curtain.

3. Reproduction Calculation Using Cloud-Resolving Model

The purpose of this chapter is to obtain reconstructions of the heavy rainfall over northern Kyushu in 2017 using the CReSS (Cloud-Resolving-Storm-Simulator), which is one of the mesoscale numerical atmospheric models. The objective is to obtain data that can be used as initial and lateral boundary conditions for calculations with a manipulated wind field assuming Offshore Curtain.

3.1 Setting Calculation Conditions

In this study, CReSS (Cloud Resolving Storm Simulator; Tsuboki (2023)) was used to simulate the torrential rainfall in northern Kyushu. The model setup is summarized in Table 3.1. Hereafter, time means Japan Standard Time (JST) unless otherwise noted. In the initial phase of the study, the start time of the replicated calculations was 09:00 on 2017/07/05. The actual start time of the heavy rainfall in the target case is 12:00, but the computation was performed a little earlier in order to track the particles that bring the precipitation, which is the aim of this study. To reproduce heavy rainfall in line shaped convective system's rainfall, it was considered necessary to have a high horizontal resolution, and a horizontal resolution of 1 km was set to achieve relatively high resolution. Because airflow is generally complex in the lower layers due to the influence of topography, a vertical grid width of 100 m was set at the lowest layer, and the vertical grid width increased as one moved up to the upper layers, reaching approximately 320 m at the uppermost layer. As a result, no rainfall was formed in this calculation which reproduced the heavy rainfall in northern Kyushu. In addition to this reproduction computation, other reproduction computations were performed with a slightly different computational range and with a 500 m mesh, but in all of them, either no rainfall area was formed or only a weak rainfall area was formed. This computation set up and other downscaled computations are summarized in Appendix A. Therefore, we decided to use the computational conditions of the ensemble forecast experiment conducted in Yamaguchi et al. (2018) using the BGM ensemble method for the torrential rainfall in northern Kyushu, Japan. The same computational model CReSS was used in this ensemble experiment, and the model settings are summarized in Table 3.1. In the study by Yamaguchi et al. (2018), there were 30 ensemble members, and in this study, we used member 015, which has been evaluated as forming a heavy rainfall that appears to be a line shaped convective system.

Table 3.1 Model Settings for CReSS

Table 3.1 Model settings for CReSS

accounting period	2017 0705 1200JST - 1800JST
Initial and Boundary Values	MSM analysis value
sea surface temperature	NEAR-GOOS (20170705)
topographic data	G topo
Horizontal resolution	1000m
vertical resolution	Average 250m
lattice parameter	500 (east-west) x 450 (north-south) x 61 (vertical)
Version of CReSS used	CReSS2.3

3.3 Checking the reproducibility of line shaped convection systems

To verify the reproducibility of the line shaped convective system, the results of the CReSS reproduction computations are shown in Fig. 3.2. The figures show the precipitation intensity during the same period of the CReSS reproduction results every 20 min from 1540 to 1700 JST. The figure shows the formation of a linear precipitation area. To confirm whether this rainfall is a line shaped convective system with a back-building structure, the mixing ratios of aqueous materials are depicted in Fig. 3.3 in a three-dimensional view. Fig. 3.4 shows the convergence and divergence at an altitude of 570 meters. It can be seen that there is convergence in the upstream of the precipitation area at each period. The above confirms that the calculation used in this study is for a line shaped convective system of torrential rainfall with a back-building structure, which is the target of the study. In the following sections, the changes and mechanisms of the installation of Offshore Curtains for this computation set up will be discussed.

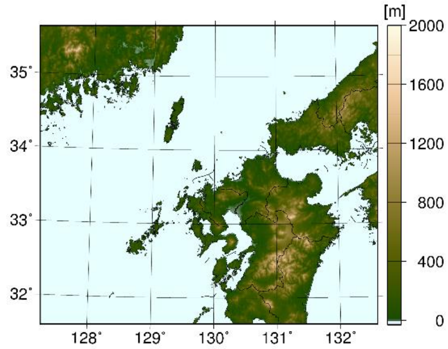

Fig. 3-1 The computation domain of CReSS

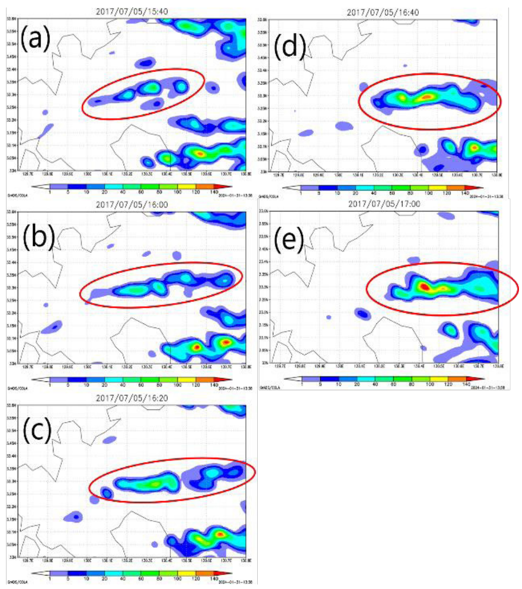

Fig. 3-2 The rainfall intensity from the initiation of the line shaped convective system at (a) 15:40, (b)16:00, (c)16:20 ,(d) 16:40 (e) 17:00

4. Calculation Scheme and Setup of Wind Field Operation

In this chapter, how to reduce heavy rainfall for the reproduced calculations analyzed in the previous chapter, along with the Offshore Curtain assumed as a weather control device is described is discussed. Section 4.2 describes the scheme of the wind speed field experiment using the cloud resolving model CReSS by Tsuboki (2023). Section 4.3 describes the wind speed field grid to be manipulated is explained, and the setup of the sensitivity experiment is also described. Offshore Curtains are barriers woven of UHMW-PE (Ultra High Molecular Weight Polyethylene), which are so light that, with a kite system at sea, the aerodynamic lift from atmospheric winds can lift and maintain the curtains. The purpose of implementing Offshore Curtains is to reduce the inflow of water vapor, wind convergence, and upwelling, which are considered important factors in the generation of heavy rainfall in line-shaped convective systems. At this stage, the suppression plan is to install the marine curtain for the prevention of inflow of water vapor. In the Northern Kyushu heavy rainfall case, the water resource to sustain the system was carried by westerly wind and to build barrier in front of the updrafts area to weaken the convergence and suppress the updrafts. In Northern Kyushu heavy rainfall, the updrafts occurred because of convergence of air behind the Seburi mountain. It should be added that although it is called Offshore Curtain, it can be installed on land as well as on the sea.

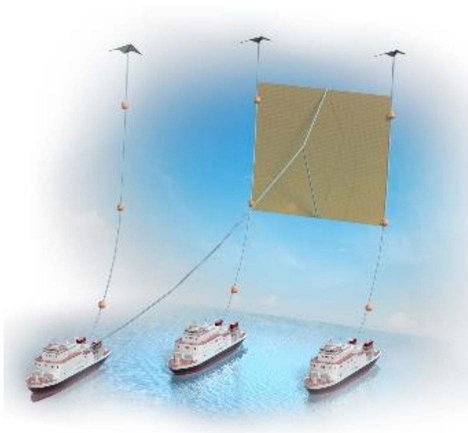

Fig. 4-1
Offshore Curtain image

4.1 Schemes for wind field operation

4.1.1 Calculation setup for wind field operations

The direct method used in this study in assuming Offshore Curtain is to manipulate the wind speed field. Although direct changes in the wind speed variable could be considered, this study decided to use the wind turbine resistor scheme, which is widely used as a resistor scheme for wind. Specifically, we adopted the Porous Disk Model of Uchida et al. (2020) and introduced the following scheme. The external force term Fi in the wind speed calculation equation in CReSS expressed in eq. (4.1). The new external force term F_i' is the wind speed squared term multiplied by an appropriate coefficient and subtracted from the external force term. The wind speed u_i is calculated as in eq. (4.2).

$$u_i = u_i + (\frac{F_i}{\rho_z}) \quad (4\text{-}1)$$

$$u_i' = u_i + \left(\frac{F_i'}{\rho_z}\right),$$

$$\text{where} \quad F_i' = F_i - C_{rc} \cdot u \cdot \sqrt{u^2 + v^2 + w^2} \quad (4\text{-}2)$$

Note that the integration time dt is 1.0 s. Here, as shown in eq. (4.2), the external force term F_i' depends on the integration time, the thrust coefficient C_{rc} must be adjusted to a realistic value. In the present operation, the thrust coefficient C_{rc} is set to 0.1. The validity of this value is discussed in the next section. As mentioned in Section 4.1, the size of the Offshore Curtain is considered to be 1 km square. The horizontal resolution of CReSS is 1 km (east-west) by 1 km (north-south), which means that the horizontal direction is represented by a single grid. The vertical resolution of CReSS is approximately 250 m, which means that the vertical direction is represented by four grids. Since the main wind direction on the upwind side of the heavy rainfall area was westerly in this subject case, this scheme was applied only to the east-west component (i = 1) in this case.

4.1.2 Effects of wind field manipulation

Verify the changes in wind velocity field and water vapor movement around the Offshore Curtain using the calculation setup described in the previous section. Fig. 4.2-4.4 compares the wind speed field without and with wind speed field operation. The wind speed field is also changing around the operating area indicated by the square. The east-west wind speed u is 4 m s^{-1} at the installation site, and the upstream wind speed, which is considered to be unaffected by the Offshore Curtain, is 10 m s^{-1}, indicating that the wind speed was reduced by about 60 %. This percentage refers to the transmission rate of the Offshore Curtain. Future verification is needed to consider the material and weave of the Offshore Curtain in the future. Compared to the results without operation, a wind speed reduction area of about 25 km is confirmed for the flow direction. This is thought to be because the weakening of wind speed at one point is propagated around the area over time within the calculation scheme. Other changes in the wind speed field include not only a weakening of the wind speed in the east-west direction, but also an increase in the wind speed vertically upward around the operating range. This is thought to be due to the horizontal convergence of the wind blowing into the Offshore Curtain, which is weakened by the Offshore Curtain, and as a result, the air mass that was supposed to escape in the east direction rises and escapes upward.

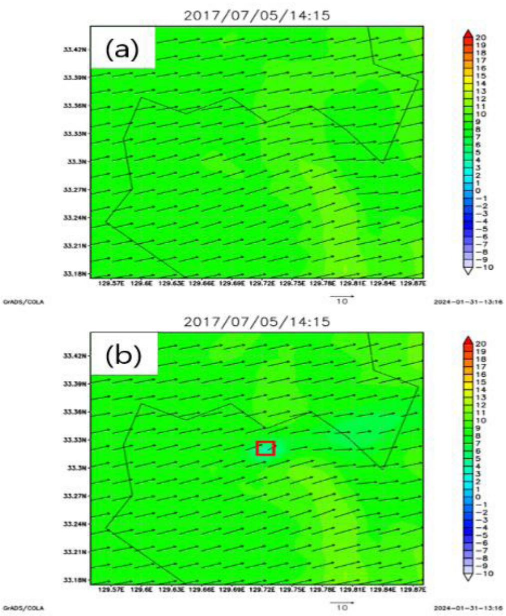

Fig. 4-2: (a) is without wind field manipulation, (b) is with curtain. The vectors are the two components of wind speed in the east-west and south-north directions, and the shading is also the wind speed in the east-west. The area enclosed by the red square is the area that was manipulated in this calculation.

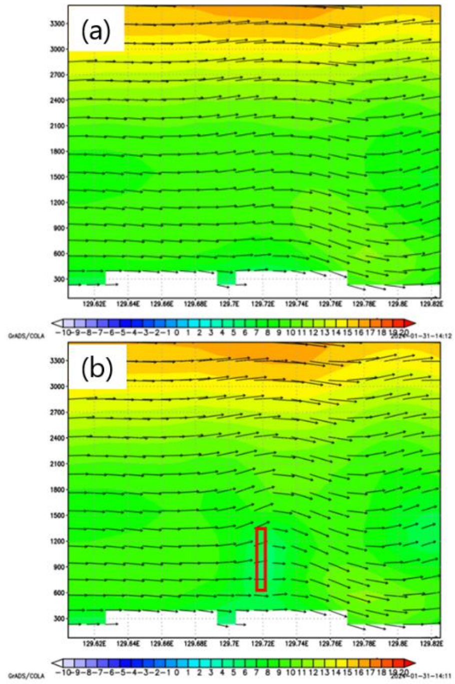

Fig. 4-3: Upper figure is without wind field manipulation; lower figure is with curtain. The vectors are the two components of wind speed in the east-west and vertical directions, and the shading is also the wind speed in the east-west. The area enclosed by the red square is the area that was manipulated in this calculation.

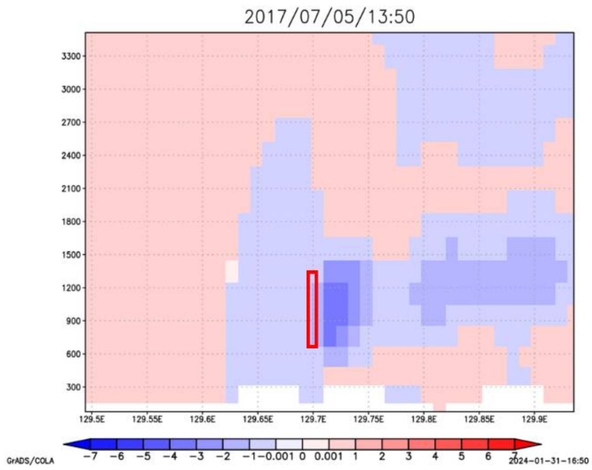

Fig. 4-4: The shade is the wind speed difference in the east-west directions. Blue color means the wind speed decreased by wind field manipulation. The area enclosed by the red square is the area that was manipulated in this calculation.

4.2 Determination of wind field operation position

In this study, numerical experiments are conducted under the wind field manipulation scheme described in the previous section, but as described in 4.1, the wind field manipulation will only be performed over a 1 km cubic area. An important aspect of the installation of the Offshore Curtain for the purpose of actual heavy rainfall control is the location at which the Offshore Curtain will be installed. Section 4.2 describes the method used to determine the location of the curtain, and the results are discussed in Section.

4.2.1 Streamline Tracking

To address the question of where to place the Offshore Curtain, the authors of this study focused on a method called stream-tracking. This method was used in Murase (2023) and is used to track the origin of water vapor. The specific formula is shown in eq.(4.3-4.5).

$$x_n(t+\Delta t) = x_n(t) + u(x_n, y_n, z_n) \cdot \Delta t \qquad (4\text{-}3)$$
$$y_n(t+\Delta t) = y_n(t) + v\,(x_n, y_n, z_n) \cdot \Delta t \qquad (4\text{-}4)$$
$$z_n(t+\Delta t) = z_n(t) + w(x_n, y_n, z_n) \cdot \Delta t \qquad (4\text{-}5)$$

In the above expression, x_n, y_n and z_n represent the eastward position (positive in the eastward direction), the north-south position (positive in the In the above expression, x_n, y and z_n represent the eastward position (positive in the northward direction), the north-south position (positive in the eastward direction), and the vertical position (positive in the upward direction) of air parcels, respectively, for any given time t and for any If Δt is positive, it is called forward trajectory and if Δt is negative, it is back trajectory. In my research, back trajectory is often used because I want to chase the origin of water vapor. To do so, we will look back at the" a line-shaped convective system generated by the no-manipulation calculation" analyzed in Chapter 3. The following figure shows the expanded precipitation intensity of the line-shaped convective system in the initiation stage and vertical section of the line-shaped convective system at the point where it is occurring. The idea of controlling heavy rainfall in line-shaped convective systems with the Offshore Curtain is based on the self-organizing structure of line-shaped convective systems due to back building phenomena. as discussed in previous studies on heavy rainfall in line-shaped convective systems in Section 2.1, rainfall from preceding cumulus clouds affects the formation of subsequent cumulus clouds in a line-shaped convective system. The mechanism of their maintenance has not been qualitatively elucidated. The mechanism of their maintenance has been qualitatively elucidated. When a developed cumulus cloud brings precipitation to the ground surface, a convergence zone appears in the lower layers by generating downdrafts, which in turn generate new updrafts. When the convergence zone occurs behind the cumulonimbus cloud, the structure self-organizes and the rainfall area stagnates, resulting in heavy rainfall. This structure is also present in the figure pasted above, where the continuity of up and down flow and lower-level headwinds are seen, and new cumulonimbus clouds are formed. Based on this structure, the idea that suppressing or weakening the first cumulonimbus in a line-shaped convective system could weaken the maintenance mechanism of the subsequent cumulonimbus itself existed in the early stages of the study. Based on this idea, the water vapor to be tracked this time was the vapor that developed the first cumulonimbus cloud. Therefore, the vapor to be tracked is the area enclosed by the black square in Fig. 4.5 at 1500 JST.

Since the red square has already been determined in the previous paragraphs, we will discuss the backward tracking decision at the end. As a supplement, the computation period is 1500-1240 JST and dt = 5 s.

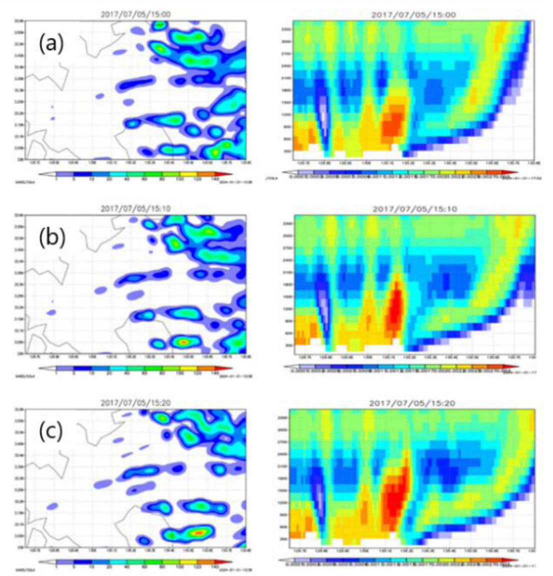

Fig. 4-5: The left figure of (a) shows rainfall intensity, the right figure are vertical section showing domain perturbation of water vaper mixing ratio (qv) at 1500 JST. Water vapor tends to be basically higher at lower elevations and lower at higher elevations. (b)-(c) are same as (a) but at 1510, 1520 JST, respectively. Therefore, to quantitatively know which location has more water vapor for all altitudes, qv, the water vapor mixing ratio minus the regional altitude average of the water vapor mixing ratio, was used as an indicator.

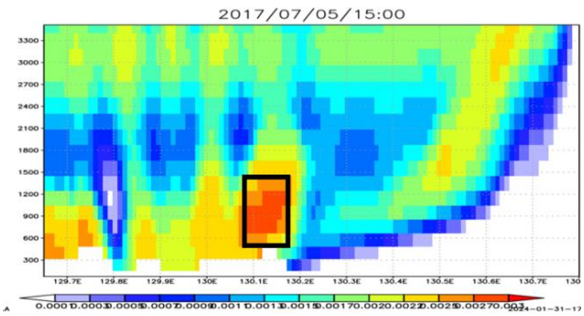

Fig. 4-6: Same as Fig. 4.5, but with the black square which indicates the domain of the initial points of the tracers.

4.2.2 Streamline Tracking Results

In this section, we analyze the results of the stream trace tracking. In this back trajectory line tracking, the tracking was initially started from the area enclosed by the black square in Fig. 4.6 in the previous section, but during the calculation, some of the water vapor collided with mountainous areas, which sometimes prevented wind speed calculation. In this calculation, Δt was set to 5 s due to the integration time. If precise tracking is the goal, the integration time should be set to 1 second, which will be a future issue. In this study, backward trajectory line tracking was performed from the front (west side) of the mountain, which is considered to be the origin of the water vapor. Fig. 4.7 below shows a bird's-eye view of the stream trace tracking results from different angles. The water vapor at the time of T=1500 JST is the area enclosed by the red square in Fig. 4.7a-b, and the water vapor at the end of the tracking is the area enclosed by the blue square. As can be read from these figures,

1. Water vapor at lower altitudes originates from the west-southwest direction.

2. The water vapor at the middle and higher altitudes originates almost due west.

Using these results as a reference, the wind speed field operation area is determined in the next section, and sensitivity experiments are set up.

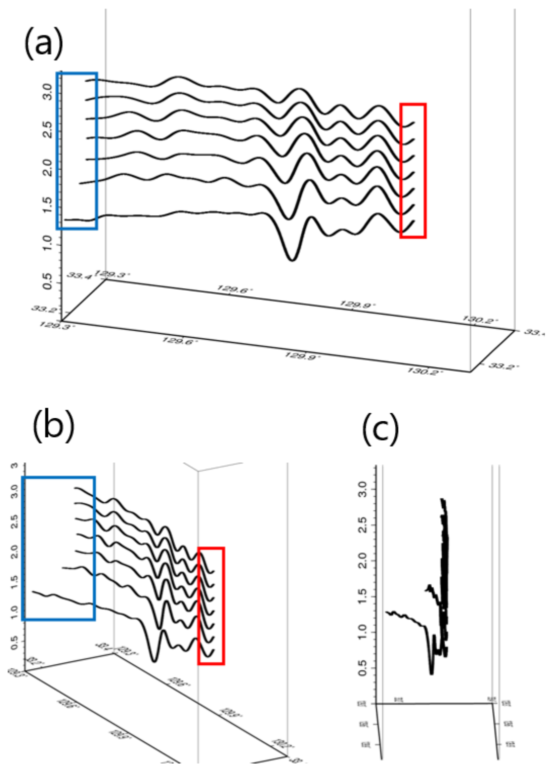

Fig. 4-7: The result of back trajectory. (a) is the result seen from south-south-east. (b) is seen from east-southeast. (c) is seen from east.

4.2.3 Determination of wind field operation area and setting up sensitivity experiment

In this section, the wind field manipulation region is determined based on the results of the backward streamline tracking described in the previous section. In this study, wind field manipulation experiments will be conducted at three altitudes with respect to the vertical direction. The lowest altitude (z =650-1450 m) is called the low layer, the middle altitude (z =1250-2080 m) the middle layer, and the highest altitude (z =1860-2750 m) the upper layer. Although the vertical calculation grid of CReSS is a major issue in setting these altitudes, we also wanted to break the origin of the water vapor in the west-southwest direction, which is one of the results of the previous section, and to make a comparison by conducting wind speed field manipulation experiments at multiple altitudes for water vapor originating almost directly west of the middle and upper layers. The objective was to compare the results of the wind speed field manipulation experiments at multiple altitudes. For the east-west direction, 16 patterns of sensitivity experiments shall be conducted every 6 km westward from the location of the first cumulus cloud. For the north-south direction, no multiple-pattern experiments were conducted, but the locations of the installations were adjusted to intercept the path of water vapor according to the results of the stream trace tracking. Under these experimental settings, sensitivity experiments were conducted in the wind field operation area. In the next chapter, we will discuss the changes in precipitation.

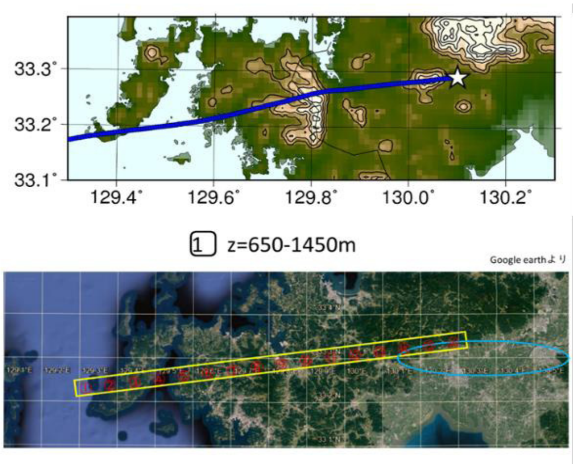

Fig. 4-8: The results of the backward flowline tracking in the lower layer together with the actual topographic data; the contour lines are filled in every 100 m, starting at 200 m. The figure below shows an image of the wind field operation locations in the lower level and their numbering.

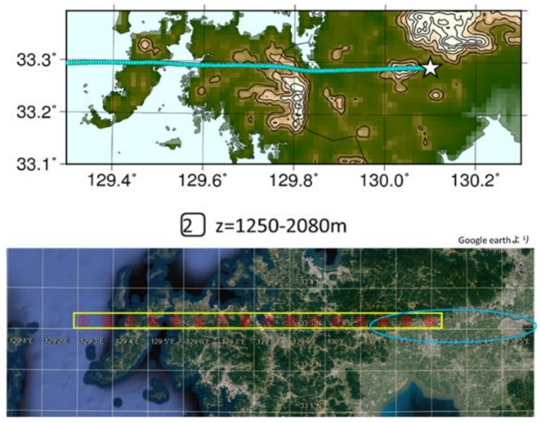

Fig. 4-9: The results of backward trajectory line tracking in the middle layer together with actual topographic data; contour lines are filled in every 100 m, starting at 200 m. The figure below shows an image of the wind field operation locations in the middle layer and their numbering.

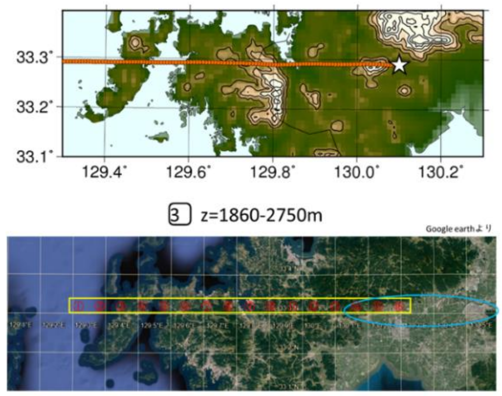

Fig. 4-10: The results of the backward trajectory line tracking in the upper layer together with the actual topographic data; the contour lines are filled in every 100 m, starting at 200 m. The lower figure shows an image of the wind field operation locations in the upper layer and their numbering.

5 Result of wind field manipulation and sensitivity experiments

In this chapter, the effects of the wind field manipulation on the line shaped convective system heavy rainfall are evaluated and the results of sensitivity experiments on the installation locations are discussed. In addition, a detailed analysis of the line-shaped convective system heavy rainfall suppressed by the wind field manipulation will contribute to the understanding of the mechanism of line-shaped convective system heavy rainfall. In Section 5.1, the spatially integrated rainfall for each sensitivity experiment is evaluated. We focus on the relationship with topography, which is considered important for line-shaped convective system heavy rainfall, in Section 5.2.

5.1 Rainfall changes in wind field manipulation experiments

In this chapter, the time-integrated rainfall amount changed by the wind field manipulation experiment is focused. To examine how the wind field manipulation changed the intensity and spatial extent of rainfall, Fig. 5.1 shows one result of the spatial distribution of the difference between the 3-hour rainfall accumulation with and without wind field manipulation. In many of the patterns, the 3-hour rainfall totals in the rainfall areas enclosed by the red squares have decreased. The intensity of the heavy rainfall areas has been dispersed and the weak rainfall areas have been widened on the leeward side and in the north-south direction, which may have mitigated the concentration of heavy rainfall in a single location. Next, in keeping with the purpose of this study, which is to control the line-shaped convective system, analysis is limited to the rainfall area within the red rectangle, and the difference in the spatial maximum of 3-hour integrated rainfall with and without the manipulation is shown in Fig. 5.2. As a result of the sensitivity experiment, the 3-hour maximum accumulated rainfall before the wind field operation was 115.2 mm, while the pattern with the wind field manipulation varied from about 76.0 mm to about 137.3 mm (-34.0 % to +19.2 %), indicating that, on average, the wind field manipulation had a” suppression” effect. It can also be read from the average values that the suppression effect was higher when installed in the lower layers. On the other hand, looking at the difference in the east-west direction, it was expected that the location closer to the rainfall area would have a greater tendency to change because of its direct effect, but this was not the case, and there were many cases where installation at some distance showed a greater suppression effect. However, there were also cases where the neighboring locations that had a large suppression effect conversely promoted an increase in rainfall. In Fig. 5.2, the comparison is based on the maximum value of 3-hour integrated rainfall. Therefore, no comparison is made for rainfall area expansion. Therefore, to examine the change in total rainfall in the line-shaped convective system next, the difference in the area-averaged 3-hour integrated rainfall is shown in Fig. 5.3 The wind field manipulation in the lower layer tends to reduce rainfall over the entire rainfall area, whereas the wind field manipulation in the middle and upper layers tends to increase rainfall over the entire rainfall area. This trend is the same as when comparing the spatial maximums in Fig. 5.3, but in more cases the increase was seen in the area-averaged case due to manipulation. Considering Fig. 5.2 and 5.3. together, there are 29 patterns in which both the mean rainfall over the rainfall area and the peak value of the 3-hour rainfall accumulated over 3 hours are decreasing, and 11 patterns in which the mean rainfall over the rainfall area is increasing but the peak value of the 3-hour rainfall accumulated over 3 hours is decreasing, indicating that there may be more than one mechanism for the decrease in the peak value of the 3-hour rainfall accumulated over 3 hours. Therefore, it is possible that multiple mechanisms cause the peak rainfall to decrease, and it is more important to clarify the mechanism of the decrease in the peak rainfall. Therefore, these 48 patterns of sensitivity experiments are not only divided into lower, middle, and upper layers but also typed by the east-west location where they were installed.

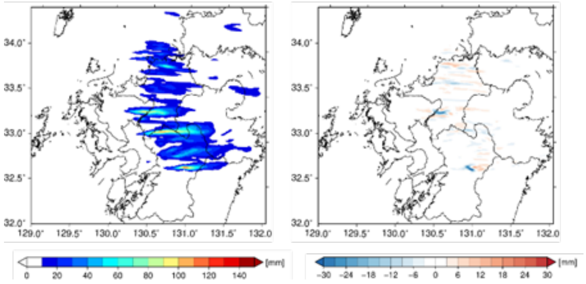

Fig. 5-1 Lefthand side figures indicate the 3-h accumulated rainfall with wind field manipulation, and righthand side figures show the difference between manipulation experiments and control run (without manipulation)

	①	②	③	④	⑤	⑥	⑦	⑧	⑨	⑩	⑪	⑫	⑬	⑭	⑮	⑯	layer average
Upper	-17.2	-14.5	-23.9	-25.4	-11.9	4.8	-5.2	10.9	-4.0	-20.5	-10.6	-1.2	-17.7	-10.6	-14.5	-20.9	-11.4
Middle	-27.1	-10.9	-34.0	-3.7	-4.3	8.5	12.0	6.5	-24.6	-18.3	-17.3	-14.2	-0.5	-5.6	-7.0	13.5	-8.0
Lower	-20.0	-31.8	-4.6	-10.4	-31.4	-34.0	-21.8	-26.9	-39.2	-31.5	-35.3	19.2	-1.5	-17.0	-3.5	-15.7	-15.1

Rainfall change by curtain for each place [mm]

decrease increase

Fig. 5-2 Difference in spatial maximum peak values of 3-hour accumulated rainfall [mm] within the rainfall area in the sensitivity experiment for the wind field manipulation operation location. Positive value means increase by manipulation, negative value means decrease by manipulation.

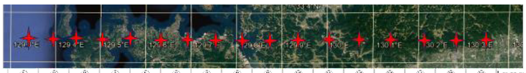

	①	②	③	④	⑤	⑥	⑦	⑧	⑨	⑩	⑪	⑫	⑬	⑭	⑮	⑯	Layer average
Upper	-1.11	-0.04	-0.68	-0.67	1.24	1.35	2.73	2.70	1.74	1.92	-0.33	0.11	-0.82	-0.75	-1.10	-1.42	0.25
Middle	0.75	0.08	0.34	1.24	2.12	1.96	2.39	1.79	0.48	0.56	0.78	0.37	0.31	0.04	0.89	0.38	0.50
Lower	-1.16	-2.39	1.70	-0.65	-0.92	-1.47	-0.89	-2.67	-2.70	-0.94	-2.40	-0.53	-0.70	-0.67	0.02	-1.21	-1.22

Area averaged rainfall change for each position [mm]

decreased -2.5 0 2.5 increased

Fig. 5-3 Difference in rainfall area averages of 3-hour accumulated rainfall [mm] in the sensitivity experiment for the wind field manipulation location. Positive value means increase by manipulation, negative value means decrease by manipulation. Red area shows the area used in average calculation

5.2 Direct effect of Offshore Curtain

In this section, the direct changes caused by wind field manipulation and their impact on the formation of cumulonimbus clouds are investigated. The changes in the wind speed field when Offshore Curtains are installed are described in Chapter 4. Fig. 5.4 shows how the small-scale wind field changes seen in Fig. 4.1-4.3 affect the water vapor flux, which represents the location of water vapor, the source of rainfall in a member with decreased precipitation. The water vapor flux shown in Fig. 5.4 starts from the curtain and decreases in the same direction as the horizontal wind velocity field. In this study, the water vapor flux is calculated by the equation

$$water\ vapor\ flux = q_v \times \sqrt{u^2 + v^2 + w^2} \qquad (1)$$

The purpose of comparing these figures is to see how the water vapor fluxes change with respect to each variable. The decrease in the water vapor mixing ratio is not spread from near the curtain to the rain area, whereas the wind speed decreases so much from the location of the curtain. In Fig. 5-5, water vapor around the curtain is a little increased (critically seen in figure (a), north and south from the decreasing area). From these results, the mechanism of the decrease in water vapor flux is due to (i) the north-south dispersion of water vapor by the curtain and (ii) the decrease in mechanical energy due to the decrease in wind velocity at the entire downstream side. Therefore, the steady decrease in the amount of water vapor flux and in particular, the steady decrease in wind speed entering the rainfall-forming region may have also reduced the overall rainfall.

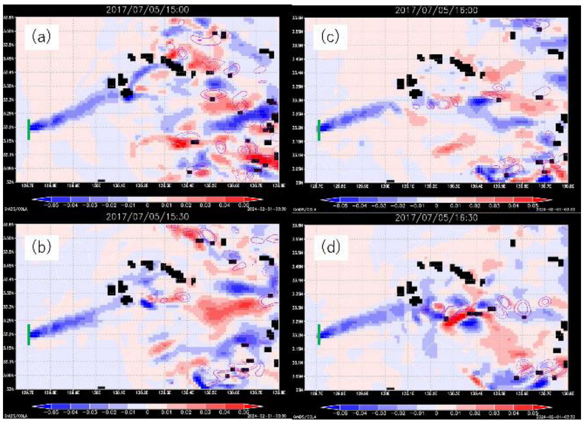

Fig. 5-4 The shading shows deference of water vapor flux [kg kg^{-1} m s^{-1}]. Blue means water vapor flux decreased because of Curtain. The line shows difference of rainfall intensity. In the case depicted by the solid line, the curtains have been installed to increase the rainfall intensity. The dotted line indicates a decrease. The green line shows the curtain location.

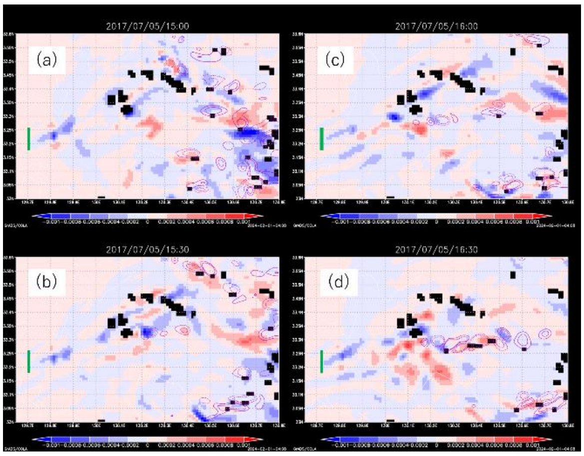

Fig. 5-5 Difference of water vapor mixing ratio [kg kg^{-1}].

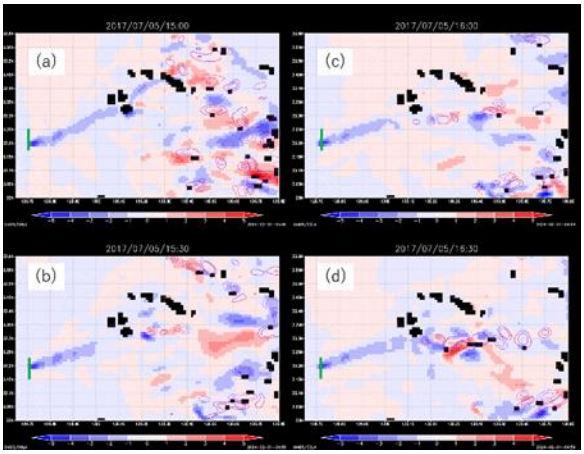

Fig. 5-6 Difference of wind speed [$m\,s^{-1}$]

6. Conclusion and Future works

The purpose of this study was to focus on the back-building structure of the line-shaped convective system and to find the possibility of controlling heavy rainfall by Offshore Curtain. Computational data reproducing the lineal convective system were obtained using the results of an ensemble experiment with perturbations created using the BGM method in the study by Horiike (2018). 48 patterns of installation locations were considered for the initial period of heavy rainfall for the line-shaped convective system. For each of these installations, wind field manipulation experiments were conducted to determine which locations could be efficiently influenced by the manipulation. The results showed that reducing the water vapor flux successfully weakened the major cumulonimbus clouds in the middle-term and late-term of the line shaped convective system, with a maximum reduction in 3-hour accumulated rainfall of 34 %. 48 patterns of sensitivity experiments showed that both rain area-averaged rainfall and peak 3-hour accumulated rainfall were reduced in 29 patterns, 11 patterns in which the rain area mean rainfall increased but the peak 3-hour accumulated rainfall decreased, and 6 patterns in which both the mean and peak values increased, indicating the possibility of heavy rainfall control even when operating in the feasible region. The wind field manipulation in the lower layer tends to reduce rainfall over the entire rainfall area. The area average rainfall intensity was reduced by 21.5 % due to lower area‘s manipulation. A more detailed analysis showed that this change was due to a weakening of the heavy rainfall in the middle of the line shaped convective system due to a reduction in water vapor flux caused by wind field manipulation. These are the conclusions as clarified in this study. For future work, we would like to take several members from the sensitivity experiment and investigate the mechanism of each precipitation change. Regarding the calculation model for the Offshore Curtain, we would like to incorporate a calculation scheme that better mimics actual effects.

Acknowledgements

This study was supported by Moonshot-type R&D project (JPMJMMS2283), Grant-in-Aid for Scientific Research 24H00291.

References

Yamaguchi, K., Nishimura, T., and Nakakita, E., 2024: Meteorological Control by Intervention in Wind Speed Field Using LES for the Guerrilla Heavy Rainfall at Toga River, Kobe, 2008, J. JSCE. B1 (Hydraulic Engineering), in press.

Yamaguchi, K., Tsuchihashi, and Nakakita, E., 2019: Analysis of the Formation of Vortex Tube and Thermals Above Urban Area by Urban Meteorological Model Based on Large Eddy Simulation. DPRI Annuals, No.62 B, 468-492.

Yokoyama, K., Onaka, T., and Suzuki, Y., 2015: Study of the Mitigating Effect on Torrential Rains and Its Mitigation Mechanism by Cloud Seeding in the Early Stage of Cloud Development. J. JSCE. B1 (Hydraulic Engineering), Vol.71, I 499-I 504.

Yagi, S., Suzuki, Y. and Yokoyama, K., 2017: Study of the Mitigation Effect and Acceleration Risk on Precipitation of Torrential Rains by Cloud Seeding with the Forced-Cooling Technique. J. JSCE. B1 (Hydraulic Engineering), Vol.73, I 259-I 264.

Tsuboki, K., 2023: High-Resolution Simulations of Tropical Cyclones and Mesoscale Convective Systems Using the CReSS Model. Park, S.K. (eds) Numerical Weather Prediction: East Asian Perspectives. Springer Atmospheric Sciences.

Yamaguchi, K., Horiike, Y. and Nakakita, E., 2018: Predictability and Development Mechanism on a Line-Shaped Rainband That Occurred at Northern part of Kyusyu in 2017. J. JSCE. B1 (Hydraulic Engineering), Vol.74, I 277-I 282.

Uchida, T., Taniyama, Y., Fukutani, Y., Nakano, M., Bai, Z., Yoshida, T. and Inui, M., 2020: A New Wind Turbine CFD Modeling Method Based on a Porous Disk Approach for Practical Wind Farm Design. Energies, Vol. 13, No. 12, 3197-1-3197-27.

Murase, K., 2023:Analysis in Role of Leading Cumulus Clouds and Water Vapor in Cumulus Cloud Development Using Terrestrial Digital Observations and Climatological Model Tracking. Master thesis (in Japanese)

(Received August 31, 2024)